Journal of Sound and Vibration (1999) **228**(3), 543–558
Article No. jsvi.1999.2427, available online at http://www.idealibrary.com on IDEAL®

DYNAMIC MODELLING AND STABILITY ANALYSIS OF AXIALLY OSCILLATING CANTILEVER BEAMS

S. H. HYUN AND H. H. YOO

Department of Mechanical Engineering, Hanyang University, Sungdong-Gu Haengdang-Dong 17, *Seoul*, 133-791 *Korea*

(*Received* 4 *February* 1999, *and in final form* 21 *May* 1999)

Dynamic stability of an axially oscillating cantilever beam is investigated in this paper. Equations of motion for the axially oscillating beam are derived and transformed into dimensionless forms. The equations include harmonically oscillating parameters which are related to the motion-induced stiffness variation. Stability diagrams of the first and the second order approximate solutions are obtained by using the multiple scale perturbation method. The stability diagrams show that there exist significant difference between the first and the second order approximate solutions. It is also found that relatively large unstable regions exist around the first bending natural frequency, twice the first bending natural frequency, and twice the second being natural frequency. The validity of the stability diagram is verified by direct numerical integrations of the equations of motion of the system.

1. INTRODUCTION

Needles of sewing machines are typical good examples of cantilever beams undergoing axially oscillating motions. Needles are usually flexible since their thickness is extremely small compared to their length. The higher the sewing quality is needed, the thinner the thickness of the needle becomes. Flexible needles may deform large considerably during the operation of sewing machines. This might cause the degradation of sewing safety as well as sewing quality. Particularly, for high-speed sewing to increase productivity, the stability of a sewing machine needle should always be guaranteed.

When cantilever beams undergo rigid body motion, their lateral bending stiffnesses often change. Typical examples are rotating beams (such as turbine and turbomachine blades). Their bending stiffnesses increase as the rotating angular speed increases. Different from the rotational motion, the axially oscillating rigid body motion results in the oscillating variation of bending stiffness. When a cantilever beam accelerates toward its free end, it is compressed and its bending stiffness decreases. On the contrary, the bending stiffness increases when the beam accelerates toward its fixed end. This variation of bending stiffness should be identified properly to accurately estimate the dynamic stability of an axially oscillating cantilever beam.

0022-460X/99/480543 + 16 $30.00/0

The study of cantilever beams undergoing rigid body motion has been mostly restricted to the case of undergoing rotational motion. When a cantilever beam undergoes rotational motion perpendicular to its axial axis, its natural frequencies as well as bending stiffness increase due to the centrifugal inertia force. References [1–4] are just some of many related papers. In references [5, 6], a dynamic modelling method for cantilever beams undergoing general rigid body motion is suggested, but its examples are restricted to rotational motion. Thus, it can be said that only rotational rigid body motion has been studied by many researchers but that translational rigid body motion such as axially oscillating motion, which is treated in this paper, has been rarely studied so far.

Systems that contain time-dependent parameters in their governing equations of motion are often called parametrically excited systems. The study of the parameterically excited system was introduced early in reference [7], and the fundamental mathematical bases were established in references [8, 9]. Since then, a large number of papers related to the topic have been published. Among them, there exist several papers focusing on methods for analyzing parametrically excited systems. In references [10–12], the Hill's method of infinite determinants was investigated. This method has been proved to be relatively inefficient when applied to systems having multiple degrees of freedom. Furthermore, it is very difficult to obtain the combinatory resonance regions by this method. In references [13–16], the Floquet's method was studied. This method is the most general one and the combinatory resonance regions as well as the principal resonance regions could be obtained with the method. However, a large amount of computational effort is required for this method. In reference [17–19], the perturbation method was studied. This method is limited to cases of small parametric excitation. By this method, the combinatory resonance regions as well as the principal resonance regions could be obtained. Furthermore, the analytical equations of the transition curves which divide the unstable and stable regions can also be obtained.

In addition to the subject of analyzing methods for parametrically excited systems, several structural dynamics problems have been studied. Stationary structures undertaking harmonic force (see, references [20, 21]), a flying structure undertaking pulsating thrusts (see, reference [22]), structures undergoing rotational motion (see, references [23–25]) and a mechanism having a flexible link (see, reference [26]) were some of the stability analysis problems of structures. The stability analysis problem of a cantilever beam undergoing axially oscillating motion, however, has not been solved in the literature. Furthermore, in most of the previous studies (for structural dynamics problems), only the first order approximate solutions were obtained. The significance of the second order solution has been rarely highlighted in structural dynamics problems.

In this paper, equations of motion for cantilever beams undergoing axially oscillating motion are derived. These equations are found to be completely different from the ones which govern the stationary structures undertaking harmonic force or structures undergoing rotational motion. The derived equations are then transformed into dimensionless forms. Two dimensionless parameters are identified from the dimensionless equations: dimensionless oscillating frequency and dimensionless oscillating speed. Once these two parameters are given, the

characteristics of the system can be determined. In order to investigate the stability of the system, the method of multiple scales (see reference [27]) is employed in this study. The stability diagrams of the first and the second order approximate solutions are obtained with the method. It is found that there exists significant differences between the first order approximate solution and the second order solution. The integrity of the stability diagram is finally confirmed by the direct numerical integration method. The stability diagram obtained in this study can be used for the design of axially oscillating cantilever-type structures such as needles in sewing machines.

2. EQUATIONS OF MOTION

In this section, the equations governing the planar motion of an axially oscillating cantilever beam are derived. The modelling method introduced in reference [6] along with Kane's method (see reference [28]) is employed for the derivation of equations of motion. The method was proved to accurately capture the motion-induced stiffness variation.

Figure 1 shows a cantilever beam which is fixed at an oscillating rigid base (denoted as A). When the beam is deformed due to the oscillating motion, the generic point (denoted as P_o) of the beam moves to a new position (denoted as P). In the figure, $\hat{\mathbf{a}}_1$ and $\hat{\mathbf{a}}_2$ represent unit vectors which are attached to the rigid base A. x is the length from the point O to the point P_o, $\mathbf{u}$ is the elastic deformation vector, and s is the stretch of the beam at point P. In conventional modelling methods, u_1 which is the $\hat{\mathbf{a}}_1$ measure number of $\mathbf{u}$ is employed instead of s. The use of the stretch variable s is one the key feature of the modelling method introduced in this paper.

To derive the ordinary differential equations of motion of the beam, s and u_2 are approximated as follows:

$$s = \sum_{k=1}^{\mu} \phi_{1k}(x) q_k(t), \tag{1}$$

$$u_2 = \sum_{k=1}^{\mu} \phi_{2k}(x) q_k(t), \tag{2}$$

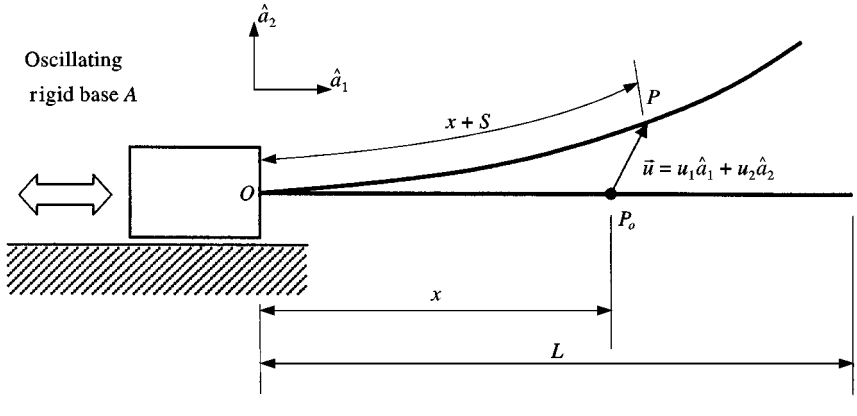

Figure 1. Configuration of axially oscillating cantilever beam.

where $\phi_{1k}(x)$ and $\phi_{2k}(x)$ are stretching and bending mode functions, q_k's are generalized co-ordinates, and μ is the total number of generalized co-ordinates. It seems that s and u_2 are involved with the same generalized co-ordinates. Actually, they do not share the same generalized co-ordinates. For instance, ϕ_{1k} is not zero only if $k \leqslant \mu_1$, and ϕ_{2k} is not zero only if $\mu_1 \leqslant k \leqslant \mu_1 + \mu_2$. In other words, μ_1 and μ_2 denote the actual number of co-ordinates for s and u_2 respectively. Thus, μ is the sum of μ_1 and μ_2.

Since rotational motion is not involved in the system of concern, the velocity of the generic point P can be easily obtained by using the following equation:

$$\mathbf{v}^P = \mathbf{v}^O + \mathbf{v}^{P/A}, \tag{3}$$

where $\mathbf{v}^O$ is the velocity of the fixed point O on the rigid base A, and $\mathbf{v}^{P/A}$ is the velocity of the point P relative to the rigid base A. In component form, they can be expressed as

$$\mathbf{v}^O = v_1 \hat{\mathbf{a}}_1, \tag{4}$$

$$\mathbf{v}^{P/A} = \dot{u}_1 \hat{\mathbf{a}}_1 + \dot{u}_2 \hat{\mathbf{a}}_2, \tag{5}$$

where dots over symbols denote time derivatives. Thus,

$$\mathbf{v}^P = (v_1 + \dot{u}_1)\hat{\mathbf{a}}_1 + \dot{u}_2 \hat{\mathbf{a}}_2. \tag{6}$$

The acceleration of the generic point, which is denoted by $\mathbf{a}^P$, can be obtained by differentiating equation (6) with respect to time:

$$\mathbf{a}^P = (\dot{v}_1 + \ddot{u}_1)\hat{\mathbf{a}}_1 + \ddot{u}_2 \hat{\mathbf{a}}_2, \tag{7}$$

u_1 must be expressed with respect to s and u_2, that are approximated in equations (1) and (2). The following geometric relation (see reference [29]) is used for the purpose:

$$x + s = \int_0^x \sqrt{(1 + u_{1,\sigma})^2 + (u_{2,\sigma})^2}\, \mathrm{d}\sigma, \tag{8}$$

where $u_{1,\sigma}$ and $u_{2,\sigma}$ denote partial differentiations of u_1 and u_2 with respect to a dummy variable σ respectively. Using Taylor's series expansion, equation (8) can be expressed as follows:

$$s = u_1 + \frac{1}{2}\int_0^x (u_{2,\sigma})^2\, \mathrm{d}\sigma + \text{H.D.T.}, \tag{9}$$

where H.D.T. denotes the higher degree terms of the expansion. Since the linear equations of motions are to be derived in the modelling method presented in this paper, the higher degree terms can be truncated without affecting the integrity of the modelling method. Neglecting the higher degree terms and differentiating

equation (9) with respect to time, the following relation can be obtained:

$$\dot{u}_1 = \dot{s} - \int_0^x (u_{2,\sigma})(\dot{u}_{2,\sigma})\,\mathrm{d}\sigma. \tag{10}$$

From equation (10) along with equation (6), the partial derivatives of $\mathbf{v}^P$ with respect to $\dot{q}_k$ are obtained as follows:

$$\frac{\partial \mathbf{v}^P}{\partial \dot{q}_k} = (\phi_{1k} - \phi_{1k}^*)\hat{\mathbf{a}}_1 + \phi_{2k}\hat{\mathbf{a}}_2, \tag{11}$$

where

$$\phi_{1k}^* = \sum_{m=1}^{\mu} \left[\int_0^x \phi_{2k,\sigma}\phi_{2m,\sigma}\,\mathrm{d}\sigma \right] q_m. \tag{12}$$

Now, the generalized inertia forces (see reference [28]) can be obtained from the following equation:

$$F_k^* = -\int_0^L \left(\rho \mathbf{a}^P \cdot \frac{\partial \mathbf{v}^P}{\partial \dot{q}_k} \right) \mathrm{d}x, \tag{13}$$

where L denotes the length of the beam, and ρ denotes mass per unit length of the beam.

By neglecting all other effects (such as shear and torsion) except stretching and bending, the strain energy of a beam can be expressed as follows:

$$U = \frac{1}{2}\int_0^L EA(s_{,x})^2\,\mathrm{d}x + \frac{1}{2}\int_0^L EI(u_{2,xx})^2\,\mathrm{d}x, \tag{14}$$

where E, A, and I denote Young's modulus, cross-sectional area, and the second area moment of inertia respectively. In the system of concern, only axially oscillating motion is prescribed and no external force is applied to the beam. Thus, the generalized active forces (see reference [28]) can be obtained from the following equation:

$$F_k = -\frac{\partial U}{\partial q_k}. \tag{15}$$

Finally, by linearizing the generalized inertia and active forces obtained in equations (13) and (15), the linearized equations of motion of axially oscillating cantilever beams are obtained as follows:

$$\sum_{m=1}^{\mu} [M_{km}^{11}\ddot{q}_m + K_{km}^S q_m] = P_k, \tag{16}$$

$$\sum_{m=1}^{\mu} [M_{km}^{22}\ddot{q}_m + (K_{km}^B - \dot{v}_1 K_{km}^G) q_m] = 0, \tag{17}$$

where

$$M_{km}^{aa} = \int_0^L \rho \phi_{ak} \phi_{am} \, \mathrm{d}x, \tag{18}$$

$$K_{km}^{S} = \int_0^L EA \phi_{1k,x} \phi_{1m,x} \, \mathrm{d}x, \tag{19}$$

$$K_{km}^{B} = \int_0^L EI \phi_{2k,xx} \phi_{2m,xx} \, \mathrm{d}x, \tag{20}$$

$$K_{km}^{G} = \int_0^L \rho (L - x) \phi_{2k,x} \phi_{2m,x} \, \mathrm{d}x, \tag{21}$$

$$P_k = -\dot{v}_1 \int_0^L \rho \phi_{1k} \, \mathrm{d}x. \tag{22}$$

equations (16) and (17) represent the governing equations for stretching motion and bending motion respectively. Since equations (16) and (17) are not coupled, they can be solved independently. The stability of the stretching motion can be simply guaranteed unless the frequency of the oscillating motion matches with one of the stretching natural frequencies, which are usually very high compared to the bending natural frequencies. For slender beams, the lowest stretching natural frequency is much larger than a few lowest bending natural frequencies. So the instability of the bending motion usually occurs before that of the stretching motion occurs. Thus, the stability of bending motion of the axially oscillating beam which is governed by equation (17) will be studied. Different from the stretching motion, the stability of the bending motion cannot be checked so easily. Since the stiffness terms in equation (17) vary as functions of time, the system of concern is an non-autonomous system. Such a system can be solved by using a stability analysis procedure which will be exhibited in the next section.

3. STABILITY ANALYSIS

For the axially oscillating motion, the axial speed v_1 can be assumed as follows:

$$v_1 = v(1 - \cos \omega t), \tag{23}$$

where v denotes the average speed of the motion. Differentiating equation (23) with respect to time, the following relation can be obtained:

$$\dot{v}_1 = v\omega \sin \omega t, \tag{24}$$

where ω denotes the frequency of the oscillating motion. Substituting equation (24) into equation (17), the following equations are obtained:

$$\sum_{m=1}^{\mu} [M_{km}^{22} \ddot{q}_m + (K_{km}^{B} - v\omega \sin \omega t K_{km}^{G} q_m] = 0. \tag{25}$$

Equation (25) represents a typical parametrically excited system since the stiffness matrix of the equation varies with time.

To obtain more general results and conclusion, equation (25) needs to be transformed into a dimensionless form. For the purpose of the transformation, the following dimensionless variables need to be introduced:

$$\xi = \frac{x}{L}, \qquad \tau = \frac{t}{T}, \qquad \vartheta_k = \frac{q_k}{L} \tag{26–28}$$

where

$$T = \sqrt{\frac{\rho L^4}{EI}}. \tag{29}$$

Using the variables introduced in equations (26)–(28), equation (25) can be written as follows:

$$\sum_{m=1}^{\mu} [M_{km}\ddot{\vartheta}_m + (\bar{K}^B_{km} - \lambda\gamma \sin \gamma\tau K_{km})\,\vartheta_m] = 0, \tag{30}$$

where a dot over a symbol now denotes the differentiation of the symbol with respect to the dimensionless time τ, and

$$M_{km} = \int_0^1 \psi_k(\xi)\psi_m(\xi)\,\mathrm{d}\xi, \tag{31}$$

$$\bar{K}^B_{km} = \int_0^1 \psi_{k,\xi\xi}\psi_{m,\xi\xi}\,\mathrm{d}\xi, \tag{32}$$

$$K_{km} = \int_0^1 (1-\xi)\psi_{k,\xi}\psi_{m,\xi}\,\mathrm{d}\xi, \tag{33}$$

$$\lambda = \frac{vT}{L}, \qquad \gamma = \omega T. \tag{34, 35}$$

The value of the function $\psi_k(\xi)$ in equation (31) is equal to that of the mode function $\phi_{2k}(x)$. The eigenfunctions of stationary cantilever beams (without oscillating motion) are used for the mode functions. Then, the mass matrix which has the components of equation (31) becomes an identity matrix, and the stiffness matrix which has the components of equation (32) becomes a diagonal matrix. Therefore, the equations of motion in equation (30) can be rewritten as follows:

$$\ddot{\vartheta}_k + \omega_k^2\vartheta_k - \varepsilon \sin \gamma\tau \sum_{m=1}^{\mu} K_{km}\vartheta_m = 0 \quad (k = 1, 2, \ldots, \mu), \tag{36}$$

where

$$\varepsilon = \lambda\gamma \tag{37}$$

and ω_k denotes the dimensionless natural frequencies of the stationary cantilever beam.

When ε in equation (36) remains small, the method of multiple scales can be applied to obtain the approximate solutions of equation (36). Transition curves, which divide the whole region into stable and unstable regions, can be obtained from the conditions to eliminate secular terms of the approximate solutions. The procedure for finding the transition curves (and drawing stability diagram) is described detailedly in reference [19], and so will not be fully repeated in this paper. Instead, the characteristic results will be summarized by considering the distinctive feature of the system of concern (axially oscillating beams) of this paper.

It is sufficient to consider up to the second order expansions in the method of multiple scales when transition curves are obtained. Therefore, equations for the first and second order transition curves will be described. The first order transition curves exist when γ is near $\omega_p + \omega_q$, and the equation for the curves can be described as follows:

$$\gamma = \omega_p + \omega_q \pm \varepsilon\sqrt{\Lambda_{pq}}, \tag{38}$$

where

$$\Lambda_{pq} = \frac{K_{pq}K_{qp}}{4\omega_p\omega_q}. \tag{39}$$

In general cases, the first order transition curves may exist when γ is near $\omega_p - \omega_q$. However, such is not true since K_{pq} is symmetric for axially oscillating beams. Therefore, the first order transition curves only exist when γ is near $\omega_p + \omega_q$.

There are several cases for the second order transition curves. The first case is when $\omega_p + \omega_q$ is near γ (this is the only case for the first order transition curves). $\omega_p + \omega_q$ is, however, away from 2γ. In this case, the equation for the second order transition curves is written as follows:

$$\gamma = \omega_p + \omega_q \pm \varepsilon\sqrt{\Lambda_{pq}} - \varepsilon^2\left\{\frac{\Lambda_{pq}}{8}\left(\frac{1}{\omega_p} + \frac{1}{\omega_q}\right) - \widehat{\chi_p} - \widehat{\chi_q}\right\}, \tag{40}$$

where

$$\widehat{\chi_p} = \frac{1}{2}\sum_{m=1}^{\mu}\omega_m\Lambda_{mp}\left[\frac{1}{(2\omega_p + \omega_q)^2 - \omega_m^2}\right] + \frac{1}{2}\sum_{m\neq q}^{\mu}\omega_m\Lambda_{mp}\left[\frac{1}{\omega_q^2 - \omega_m^2}\right], \tag{41}$$

$$\widehat{\chi_q} = \frac{1}{2}\sum_{m=1}^{\mu}\omega_m\Lambda_{mq}\left[\frac{1}{(2\omega_q + \omega_p)^2 - \omega_m^2}\right] + \frac{1}{2}\sum_{m\neq p}^{\mu}\omega_m\Lambda_{mq}\left[\frac{1}{\omega_p^2 - \omega_m^2}\right], \tag{42}$$

The second term of equation (41) represents the summation (from $m = 1$ to μ) except $m = q$, and that of equation (42) represents the summation except $m = p$.

The second case is when $\omega_p + \omega_q$ is near 2γ but away from γ. In this case, the equation for the second order transition curves is written as follows:

$$\gamma = \tfrac{1}{2}(\omega_p + \omega_q) + \varepsilon^2\{\tfrac{1}{2}(\chi_p + \chi_q) \pm \sqrt{\mu_{pq}\mu_{qp}}\} \tag{43}$$

where

$$\chi_p = \frac{1}{2}\sum_{m=1}^{\mu} \omega_m \Lambda_{mp}\left[\frac{1}{(\omega_p+\gamma)^2-\omega_m^2}+\frac{1}{(\omega_p-\gamma)^2-\omega_m^2}\right], \tag{44}$$

$$\mu_{pq} = \frac{1}{2\omega_p}\sum_{m=1}^{\mu} \frac{K_{pm}K_{mq}}{4}\left[\frac{1}{(\omega_q+\gamma)^2-\omega_m^2}\right], \tag{45}$$

where γ's inside χ_p and μ_{pq} should be replaced $\frac{1}{2}(\omega_p+\omega_q)$. In general cases, the second order transition curves may also exist around $2\gamma \approx \omega_p - \omega_q$. However, such is not true for the system of concern (axially oscillating beams).

The third case is when $\omega_p + \omega_q$ is near γ and $\omega_s + \omega_q$ is near 2γ. In this case, unlike the explicit form of above cases, transition curves can be obtained as follows. To express the nearness of γ to $\omega_p + \omega_q$ and to $(\omega_s + \omega_q)/2$, the detuning parameters are defined by

$$\gamma = \omega_p + \omega_q + \sigma_1\varepsilon, \tag{46}$$

$$\gamma = \tfrac{1}{2}(\omega_s + \omega_q) + \tfrac{1}{2}\sigma_2\varepsilon^2. \tag{47}$$

Then, transition curves are determined by the condition that λ has two equal real roots in the following equation:

$$(\lambda+\gamma_1)(\lambda+\gamma_3)(\lambda+\gamma_3) + (\gamma_4+\gamma_5)\lambda + \gamma_3\gamma_4 + \gamma_2\gamma_5 = 0, \tag{48}$$

where

$$\gamma_1 = \varepsilon\left(\frac{\Lambda}{8\omega_q} + \widehat{\chi_q}\right), \qquad \gamma_2 = \sigma_1 - \varepsilon\left(\frac{\Lambda}{8\omega_p} + \widehat{\chi_p}\right), \qquad \gamma_3 = \varepsilon(\sigma_2 - \chi_s), \tag{49}$$

$$\gamma_4 = \frac{\Lambda_{pq}}{4}\left(1-\frac{\varepsilon\sigma_1}{2\omega_p}\right)\left(1-\frac{\varepsilon\sigma_1}{2\omega_q}\right), \qquad \gamma_5 = \varepsilon^2\mu_{sq}\mu_{qs}. \tag{50}$$

From the condition of two equal real roots, σ_1 and σ_2 can be determined, and the similar procedure is given in reference [19]. However, as will be shown in the next section, this third case does not occur in our system of concern.

4. NUMERICAL RESULTS

Figures 2 and 3 show the stability diagram of the axially oscillating beams in which stable regions and unstable hatched regions are separated by transition curves. The maximum axial speed λ and the oscillating frequency γ are the two dimensionless parameters to determine the stability of the system. Figures 2 and 3 exhibit the results of applying the multiple scale method up to the first and second order respectively. Transition curves of the first order shown in Figure 2 originate from $\gamma = \omega_p + \omega_q$, and those of the second order shown in Figure 3 originate from $\gamma = (\omega_p + \omega_q)/2$ as well as $\gamma = \omega_p + \omega_q$. From these figures, it can be easily

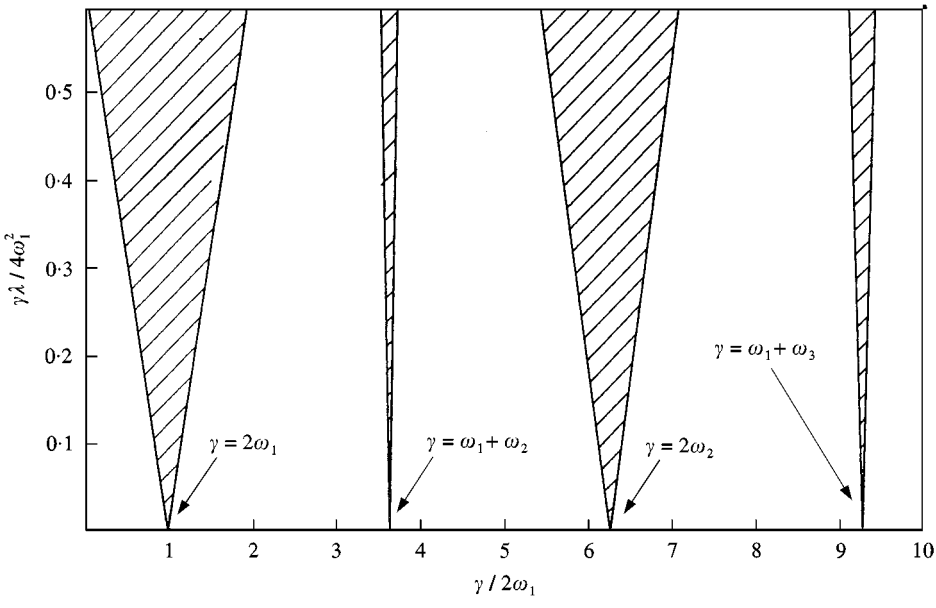

Figure 2. Stability diagram of axially oscillating beams considering up to the first order.

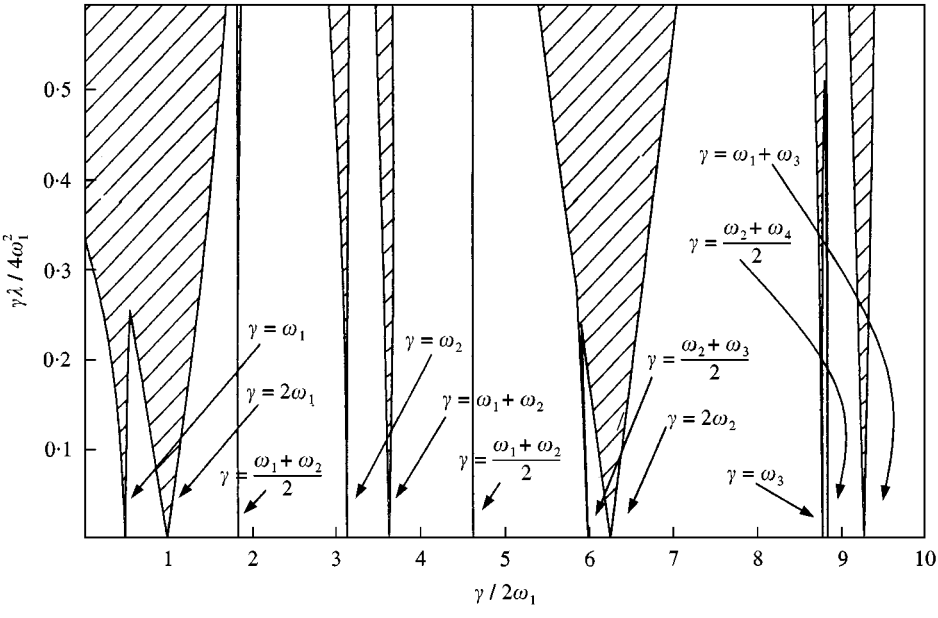

Figure 3. Stability diagram of axially oscillating beams considering up to the second order.

observed that the unstable regions which originate from $\gamma = (\omega_p + \omega_q)/2$ are relatively narrower than those originating from $\gamma = \omega_p + \omega_q$. Likewise, the unstable regions of higher than second order which exist near $\gamma = (\omega_p + \omega_q)/m$ ($m = 3, 4, 5, \ldots$) are much narrower than the first and second order regions. It is

practically impossible for the dimensionless frequency parameter to belong to the narrow unstable regions of the higher orders. Furthermore, it is well known that unstable regions retreat from the horizontal axis if damping exists (see reference [27]). Therefore, stability diagrams considering higher than second order need not be obtained. Note that even the unstable region of the second order near $\gamma = (\omega_1 + \omega_3)/2$ looks like a line. The unstable region of the second order near $\gamma = \omega_1$, however, merges with the first order unstable region near $\gamma = 2\omega_1$, and changes the original first order unstable region significantly.

In Figure 4, several points are marked in the dimensionless parameter plane, where solid lines represent the transition curves of Figure 3 and dotted lines represent those of Figure 2. For the points, equations of motion are solved by using direct numerical integration Ten mode functions are used to generate the stiffness matrix elements K_{km} in equation (36). The initial displacement and velocity of the free end of the cantilever beam is given as 0·01 and 0 respectively. Figures 5(a)–5(c) represent the simulation results of the points A, B, and C respectively. As shown in Figure 4, the points A and B belong to the unstable region, and Figures 5(a) and 5(b) show unstable dynamic responses accordingly. Note that the point A, if the results of the first order multiple scale method were used, might be presumed to belong to the stable region. The point *C* belongs to the stable region, and Figure 5(c) shows the corresponding stable dynamic response. In contrast to the point A, the point C might be presumed to belong to the unstable region if the results of the first order multiple scale method were used.

The co-ordinates of the point D in the plane of Figure 4 are (4·6, 0·5). Even though the point D seems to be located on the transition curve, it actually belongs to the stable region. Figure 6(a) shows the corresponding stable dynamic response.

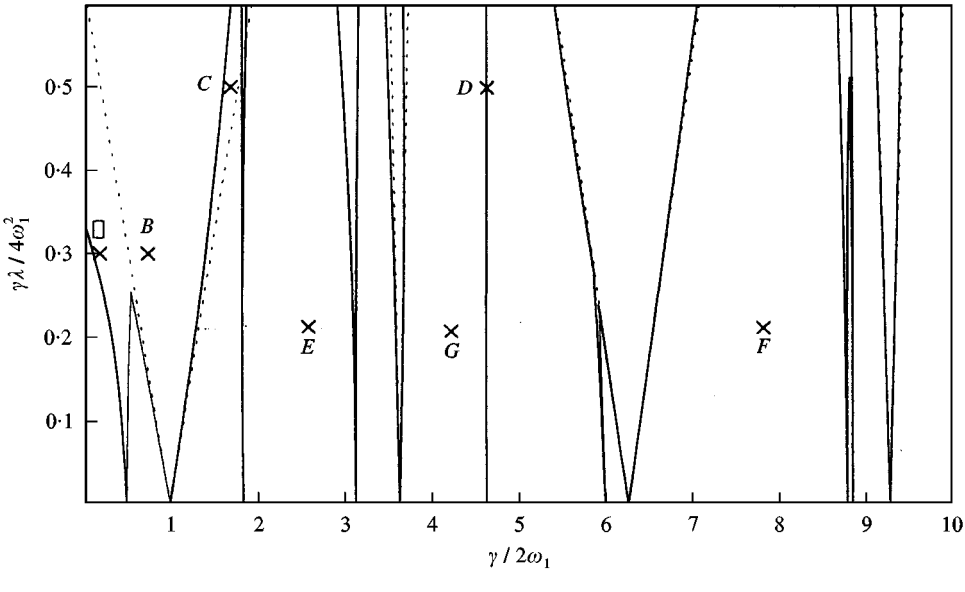

Figure 4. Points selected from the stability diagram for direct numerical integration.

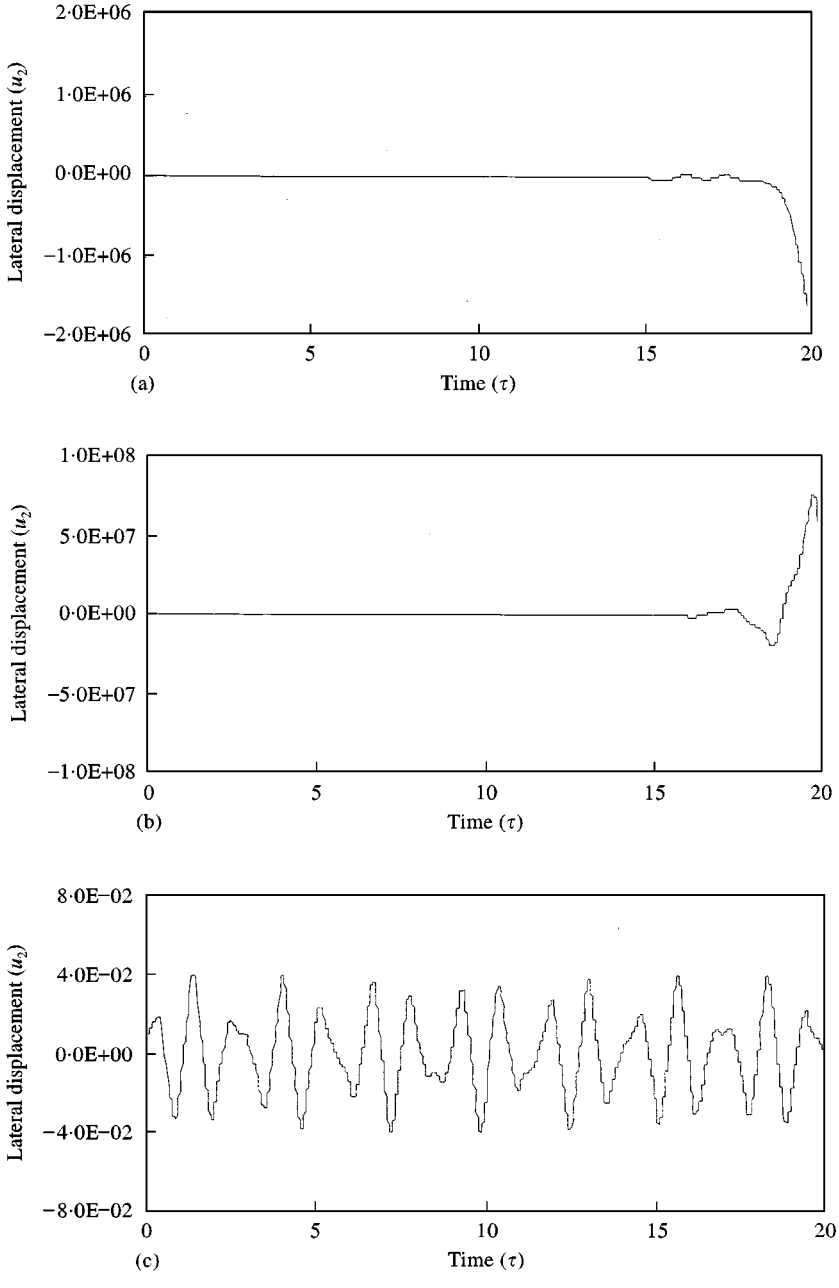

Figure 5. Numerical integration results for points A, B, C. (a) Point A with the co-ordinates of (0·2, 0·3). (b) Point B with the co-ordinates of (0·75, 0·3). (c) Point C with the co-ordinates of (1·7, 0·5).

The unstable region is so narrow around the point D that one should increase the number of digits of co-ordinates to locate an unstable point. The co-ordinates of (4·6369, 0·5) is the example of unstable point, and the corresponding results are shown in Figure 6(b). Figure 6(b) seems to show a stable dynamic response.

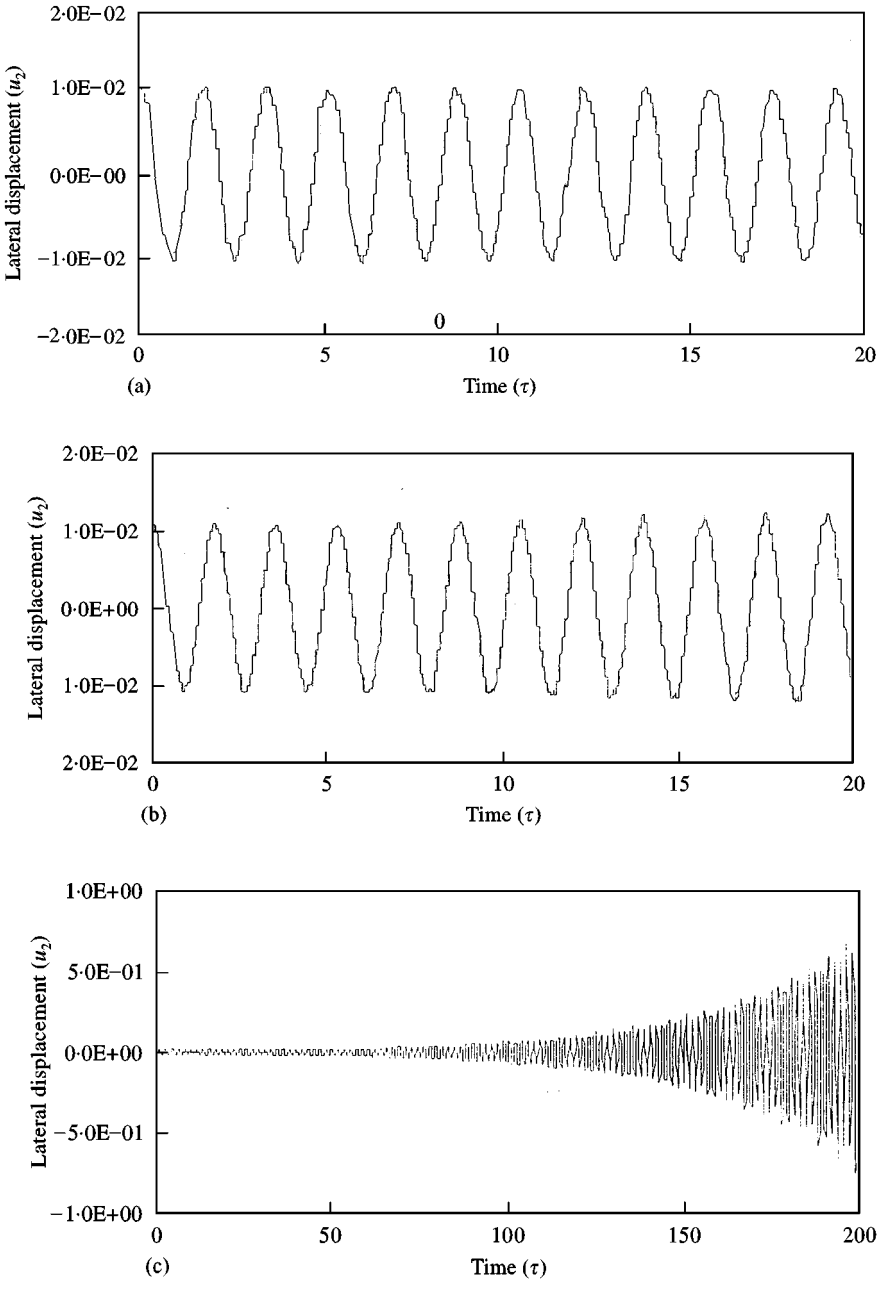

Figure 6. Numerical integration results for point D and near point D. (a) Point D with the co-ordinates of (4·6, 0·5). (b) Near point D with the co-ordinates of (4·6369, 0·5). (c) Near point D with long integration time.

Actually, the amplitude increases so slowly that one can hardly observe the diverging result unless he increases the simulation time sufficiently. Figure 6(c) shows the unstable dynamic response. However, such an unstable response would not occur in real world since even slight damping can stabilize the response.

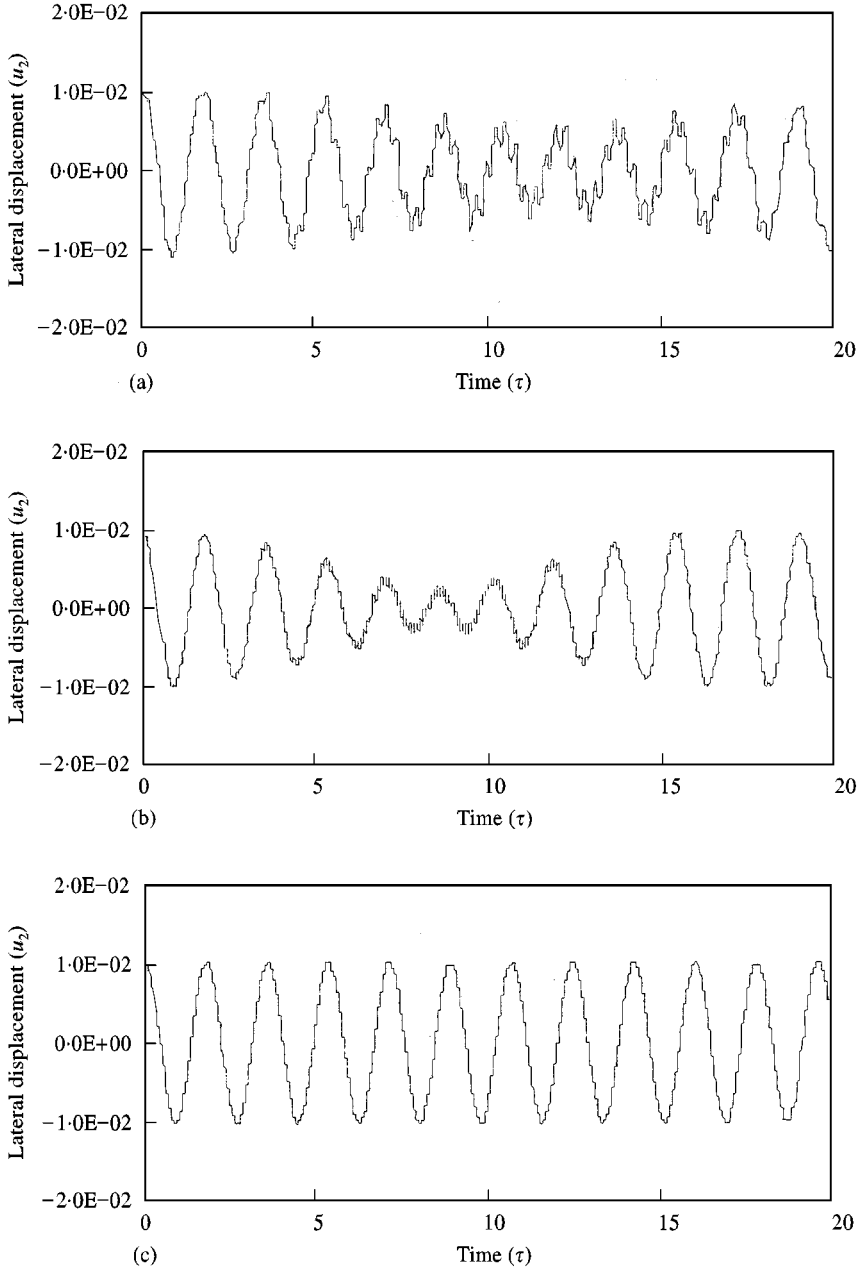

Figure 7. Numerical integration results for points E, F, G. (a) Point E with the co-ordinates of (2·6334, 0·2). (b) Point F with the co-ordinates of (8·2737, 0·2). (c) Point G with the co-ordinates of (4·1369, 0·2).

The co-ordinates of point E, F, and G shown in Figure 4 are (2·6334, 0·2), (8·2737, 0·2) and (4·1369, 0·2) respectively. The x-coordinates of point E, F, and G are equal to $\omega_2 - \omega_1$, $\omega_3 - \omega_1$, and $(\omega_3 - \omega_1)/2$. In the previous section, it was mentioned that these points have nothing to do with unstable responses in case of

axially oscillating beams. Figures 7(a)–7(c) exhibit the simulation results of points E, F, and G respectively. These results clearly confirm the validity of the conclusion made in the previous section.

5. CONCLUSION

The equations of motion of axially oscillating cantilever beams are derived by introducing and approximating a stretch variable instead of the conventional longitudinal Cartesian deformation variable. The equations include a time varying, harmonically oscillating stiffness matrix which results from the axially oscillating translational motion. Dynamic stability analysis of the system is performed by employing the multiple scale perturbation method, and the integrity of the stability diagram obtained from the analysis is verified by direct numerical integrations at several points in the plane of the stability diagram. The stability diagram shows that relatively large unstable regions exist neat the first bending natural frequency, twice the first bending natural frequency, and twice the second bending natural frequency. Other unstable regions are too narrow to be considered for actual designs. This diagram can be usefully referenced for the design of slender cantilever beam-like structures such as sewing machine needles which undergo axially oscillating translational motions.

REFERENCES

1. R. Southwell and F. Gough 1921 *British A.R.C. Reports and Memoranda No.* 766 The free transverse vibration of airscrew blades.
2. M. Schilhansl 1958 *Journal of Applied Mechanics, Transaction of American Society of Mechanical Engineers* **25**, 28–30. Bending frequency of a rotating cantilever beam.
3. S. Putter and H. Manor 1978 *Journal of Sound and Vibration* **56**, 175–185. Natural frequencies of radial rotating beams.
4. H. Yoo and S. Shin 1998 *Journal of Sound and Vibration* **212**, 807–828. Vibration analysis of rotating cantilever beams.
5. T. Kane, R. Ryan and A. Banerjee 1987 *Journal of Guidance, Control and Dynamics* **10**, 139–151. Dynamics of cantilever beam attached to a moving base.
6. H. Yoo, R. Ryan and R. Scott 1995 *Journal of Sound and Vibration* **181**, 261–278. Dynamics of flexible beams undergoing overall motions.
7. M. Faraday 1831 *Philosophical Transactions of the Royal Society* (London) 299–318. On a peculiar class of acoustical figures and on certain forms assumed by a group of particles upon vibrating elastic surfaces.
8. E. Mathieu 1868 *Journal of Mathematics* **13**, 137–203. Memoire sur ie mouvement vibratoire d'une membrane de forme elliptique.
9. G. Hill 1886 *Acta Mathematica* **8**, 1–36. On the part of the lunar perigee which is a function of the mean motions of the Sun and Moon.
10. V. Bolotin 1964 *The Dynamic Stability of Elastic Systems.* San Francisco: Holden-Day.
11. R. Brockett 1970 *Finite Dimensional Linear Systems.* New York: Wiley.
12. K. Lindh and P. Likins 1970 *AIAA Journal* **8**, 680–686. Infinite determinant methods for stability analysis of periodic-coefficient differential equations.
13. C. Hsu 1972 *Journal of Applied Mechanics* **39**, 551–558. Impulsive parametric excitation: theory.

14. C. Hsu and W. Cheng 1973 *Journal of Applied Mechanics* **40**, 78–86. Application of the theory of impulsive parametric excitation and new treatment of general parametric excitation problems.
15. C. Hsu 1974 *Journal of Mathematical Analysis and Application* **45**, 234–251. On approximating a general linear periodic system.
16. C. Hammond 1974 *Journal of American Helicopter Society* **19**, 14–23. An application of Floquet theory to prediction of mechanical instability.
17. C. Hsu 1963 *Journal of Applied Mechanics* **30**, 367–372. On the parametric excitation of a dynamic system having multiple degrees of freedom.
18. F. Fu and S. Nemat-Nasser 1973 *AIAA Journal* **10**, 30–36. Stability of solution of systems of linear-differential equations with harmonic coefficients.
19. A. Nayfeh and D. Mook 1977 *Journal of Acoustical Society of America* **62**, 375–381. Parametric excitations of linear systems having many degrees of freedom.
20. T. Iwatsubo, M. Saigo and Y. Sugiyama 1973 *Journal of Sound and Vibration* **30**, 65–77. Parametric instability of clamped–clamped and clamped–simply supported columns under periodic axial loads.
21. A. Kounadis and S. Belbas 1977 *Journal of Structural Mechanics* **5**, 383–394. On the parametric resonance of columns carrying concentrated masses.
22. T. Beal 1965 *AIAA Journal* **3**, 486–494. Dynamic stability of a flexible missile under constant and pulsating thrusts.
23. D. Peters and K. Hohenemser 1971 *Journal of American Helicopter Science* **16**, 25–33. Application of the Floquet transition matrix to problems of lifting rotor stability.
24. P. Friedmann and L. Silverthorn 1974 *AIAA Journal* **12**, 1559–1565. Aeroelastic stability of periodic systems with application to rotor blade flutter.
25. P. Friedmann and P. Tong 1973 *Journal of Sound and Vibration* **30**, 9–31. Nonlinear flap-lag dynamics of hingeless-helicopter blades in hover and in forward flight.
26. D. Beal and R. Scott 1990 *Journal of Sound and Vibration* **141**, 227–289. The stability and response of a flexible rod in a quick return mechanism.
27. A. Nayfeh and D. Mook 1979 *Nonlinear Oscillation*. New York: Wiley.
28. T. Kane and D. Levinson 1985 *Dynamics, Theory and Applications*. New York: McGraw-Hill Book Co.
29. L. Eisenhart 1947 *An Introduction to Differential Geometry*. Princeton, NJ: Princeton University Press.